Supporting Information for

Cu^{2+} recognition by N,N'-benzylated bis(amino amides)

Lingaraju Gorla, Vicente Martí-Centelles, Belén Altava,* M. Isabel Burguete and Santiago V. Luis*

Departamento de Química Inorgánica y Orgánica, Universitat Jaume I, Avda. Sos Baynat s/n., 12071 Castellón, Spain, E-mail: altava@uji.es, luiss@uji.es

S No	List of contents
Figure S1	Packing of ligand **3** found in the X-ray crystal structure
Table S1	Crystallography table of ligand **3** & Complexes **5a – 6b**
Figure S2	Distribution diagrams of ligands **2**, **3** and **4**
Figure S3	Comparison of FT-IR spectroscopy of ligand **4** and Complex **6a**
Figure S4	Comparison of UV-Visible spectra for Ni^{2+} complex with ligand **4**
Figure S5	Colorimetric image of metal recognition with different M^{2+} ions
Table S2	Change in pH of different solutions
Figure S6	Job plot of complex formation by ligand **4** with Cu^{2+}
Figure S7	UV-Vis spectra of ligand **4** with different Cu^{2+} salts
Figure S8	UV-Visible titration of Cu^{2+} with ligand **4**
Figure S9	Naked eye LOD determination of Cu^{2+}.**4** complexes after adding the 2 equivalents of base
Figure S10	LOD determination of **4**:Cu^{2+} complex from dilutions of 10 mM solution by UV-Visible experiments
Figure S11	LOD determination of Cu^{2+} from UV-Visible experiments starting for 1 mM solution of ligand **4** and adding increasing amounts of Cu^{2+} in the absence of added base
Figure S12	LOD determination of Cu^{2+} from UV-Visible experiments starting for 1 mM solution of ligand **4** and adding increasing amounts of Cu^{2+} in the presence of added base
Figure S13	LOD determination of **4**:Cu^{2+} complex from serial dilutions of a 10 mM solution of the complex by CD experiments in the absence of added base
Figure S14	LOD determination of **4**:Cu^{2+} complex from serial dilutions of a 2.5 mM solution of the complex by CD experiments in the presence of added base
Figure S15	Identification of Cu^{2+} in the presence of other metal cations using ligand **4** in the absence of added base
Figure S16	ESI mass spectra for ligand **4** in the presence of different metals
Figure S17	Distribution diagrams for the systems involving ligands **2** (a) and **4** (b) and Cu^{2+}

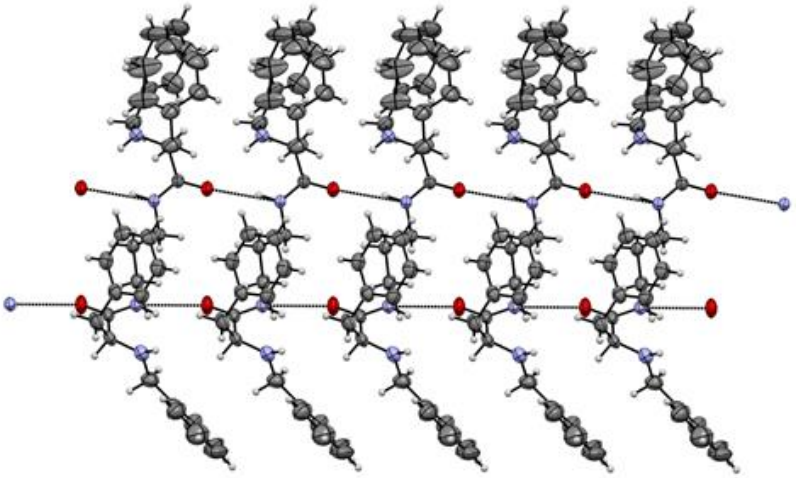

Figure S1. Packing found in the X-ray crystal structure of ligand **3**.

Identification code	**3**	**5a**	**5b**	**6a**	**6b**
Empirical formula	$C_{35}H_{40}N_4O_2$	$C_{35}H_{42}CuN_4O_4$	$C_{35}H_{42}N_4NiO_4$	$C_{27}H_{40}CuN_4O_3$	$C_{27}H_{40}N_4NiO_3$
Formula weight	548.71	646.26	641.43	532.17	527.34
Temperature/K	293(2)	297.9(6)	150.0	141(20)	199.95(10)
Crystal system	monoclinic	monoclinic	orthorhombic	orthorhombic	orthorhombic
Space group	$P2_1$	$P2_1$	$P2_12_12_1$	$P2_12_12_1$	$P2_12_12_1$
a/Å	14.9282(3)	9.6591(3)	10.35136(10)	10.8225(2)	11.0695(3)
b/Å	5.14524(8)	15.9975(4)	15.75766(13)	15.3302(3)	15.2253(4)
c/Å	19.5488(3)	10.4363(3)	19.30342(19)	16.2148(3)	16.1040(5)
α/°	90	90	90	90	90
β/°	98.3145(16)	97.225(3)	90	90	90
γ/°	90	90	90	90	90
Volume/$Å^3$	1485.75(4)	1599.82(8)	3148.64(5)	2690.22(9)	2714.11(13)
Z	2	2	4	4	4
$\rho_{calc}g/cm^3$	1.227	1.342	1.353	1.314	1.291
μ/mm^{-1}	0.602	0.727	1.250	0.846	0.749
F(000)	588.0	682.0	1360.0	1132.0	1128.0
Crystal size/mm^3	0.042 × 0.079 × 0.851	0.39 × 0.275 × 0.105	0.3663 × 0.1019 × 0.0671	0.133 × 0.173 × 0.390	0.2208 × 0.1231 × 0.0868
Radiation	CuKα (λ = 1.54184)	MoKα (λ = 0.71073)	CuKα (λ = 1.54184)	MoKα (λ = 0.71073)	MoKα (λ = 0.71073)
2Θ range for data collection/°	6.984 to 145.248	5.986 to 51.996	7.242 to 144.258	5.684 to 58.19	5.724 to 58.558
Index ranges	$-18 \le h \le 18$, $-6 \le k \le 6$, $-24 \le l \le 24$	$-11 \le h \le 11$, $-19 \le k \le 19$, $-12 \le l \le 12$	$-9 \le h \le 12$, $-19 \le k \le 19$, $-23 \le l \le 23$	$-14 \le h \le 13$, $-20 \le k \le 20$, $-20 \le l \le 21$	$-14 \le h \le 15$, $-20 \le k \le 20$, $-21 \le l \le 21$
Reflections collected	27124	30342	29035	29728	30689
Independent reflections	5829 [R_{int} = 0.0497, R_{sigma} = 0.0302]	6280 [R_{int} = 0.0647, R_{sigma} = 0.0379]	6132 [R_{int} = 0.0459, R_{sigma} = 0.0309]	6665 [R_{int} = 0.0543, R_{sigma} = 0.0466]	6801 [R_{int} = 0.0547, R_{sigma} = 0.0434]
Data/restraints/parameters	5829/488/491	6280/7/329	6132/8/421	6665/2/338	6801/2/331
Goodness-of-fit on F^2	1.021	1.036	0.948	1.095	1.062
Final R indexes [I>=2σ (I)]	R_1 = 0.0527, wR_2 = 0.1409	R_1 = 0.0361, wR_2 = 0.0917	R_1 = 0.0377, wR_2 = 0.0972	R_1 = 0.0340, wR_2 = 0.0700	R_1 = 0.0392, wR_2 = 0.0859
Final R indexes [all data]	R_1 = 0.0568, wR_2 = 0.1463	R_1 = 0.0401, wR_2 = 0.0954	R_1 = 0.0459, wR_2 = 0.1021	R_1 = 0.0408, wR_2 = 0.0738	R_1 = 0.0521, wR_2 = 0.0947
Largest diff. peak/hole / e $Å^{-3}$	0.27/-0.25	0.41/-0.29	0.71/-0.24	0.36/-0.43	0.67/-0.24
Flack parameter	0.14(19)	-0.005(7)	-0.020(10)	-0.001(5)	-0.020(6)
CCDC number	1481178	1481179	1481180	1481181	1481182

Table S1. Crystallography table of ligand **3 &** Complexes **5a–6b**.

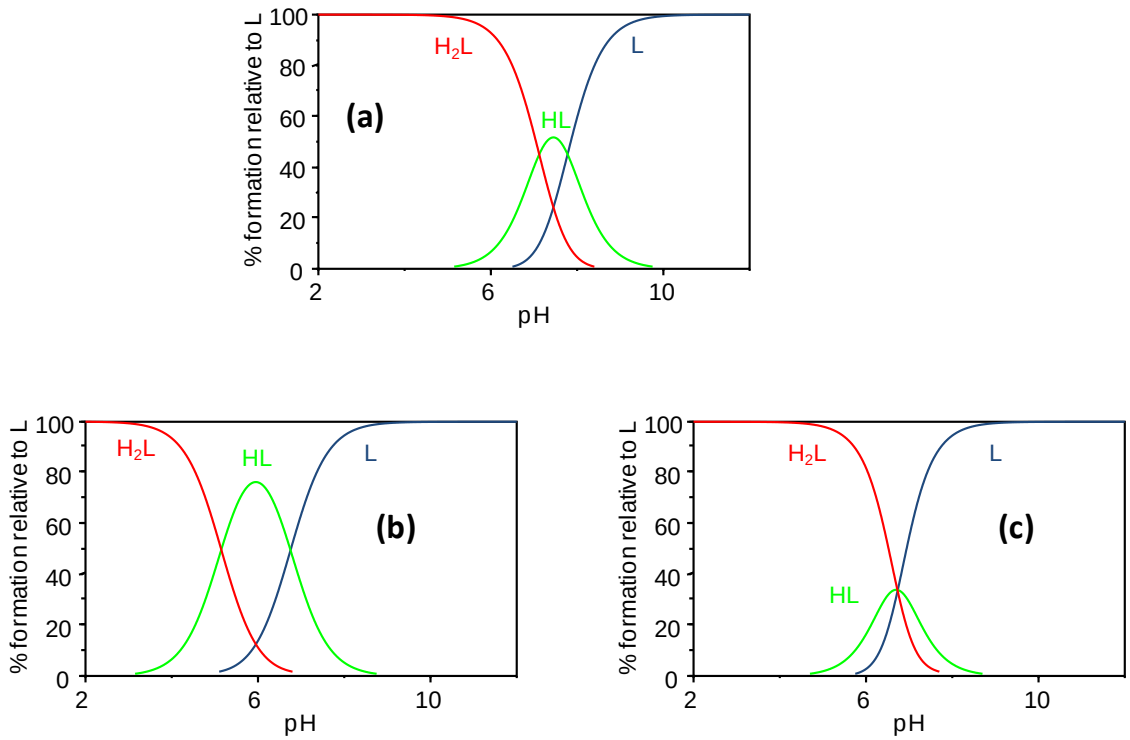

Figure S2. Distribution diagrams for the protonated species of ligand **2** (a), ligand **3** (b) and ligand **4** (c) as a function of pH in 0.1 M NaCl in H_20/CH_3CN 7/3 v/v at 298 K (1:1 stoichiometry). Charges have been omitted for clarity.

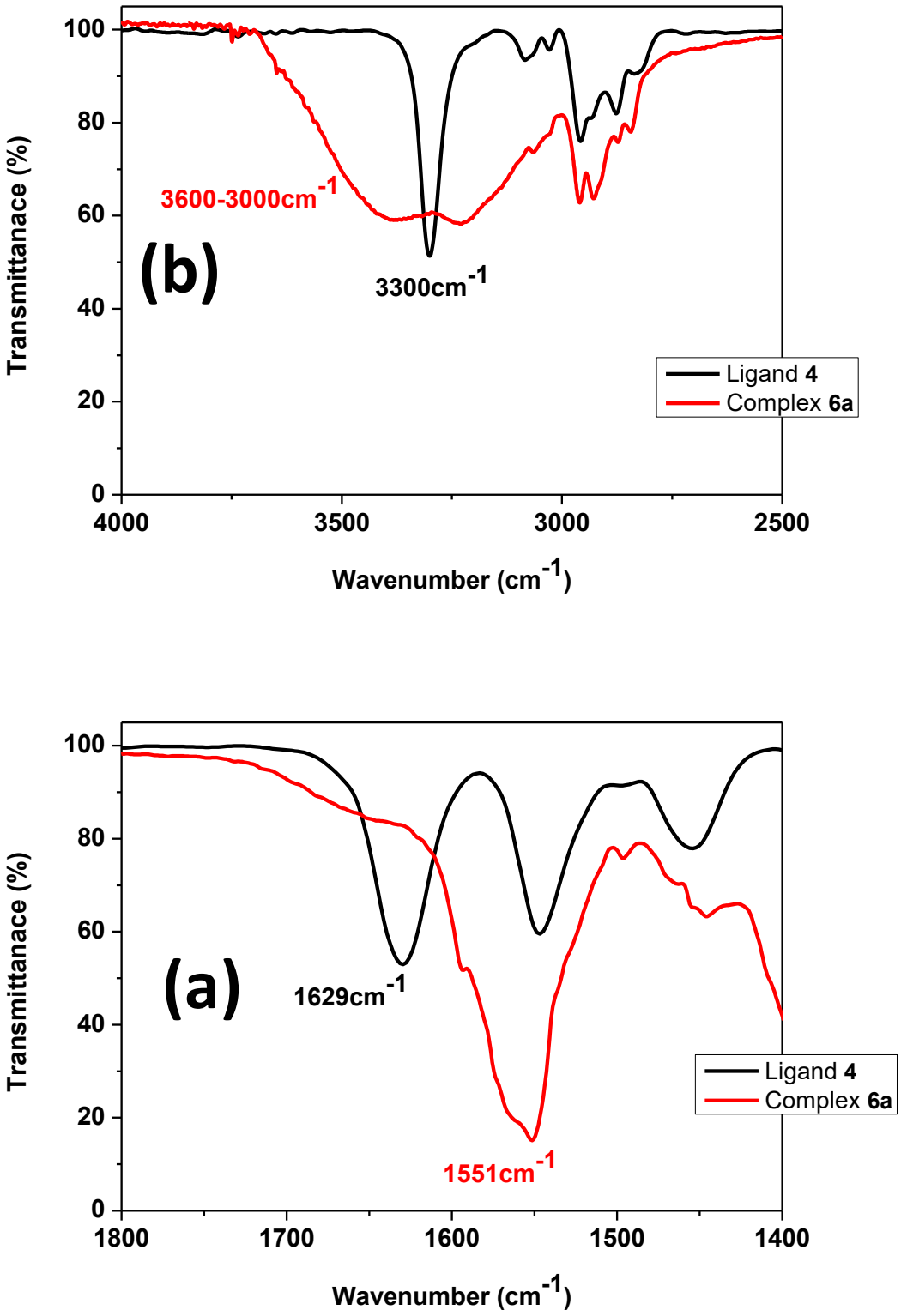

Figure S3. Comparison of selected regions of the FT-IR spectra for ligand **4** and complex **6a** (a) Change in C=O (b) Change in NH band stretching frequencies.

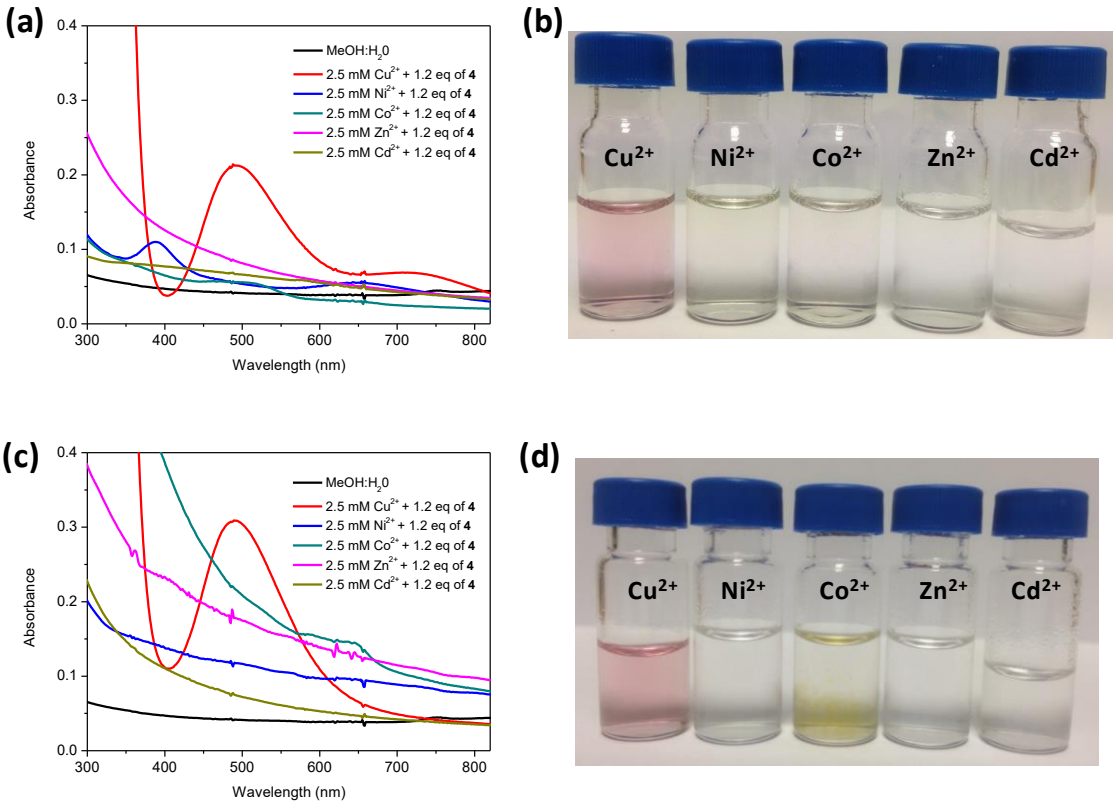

(e)

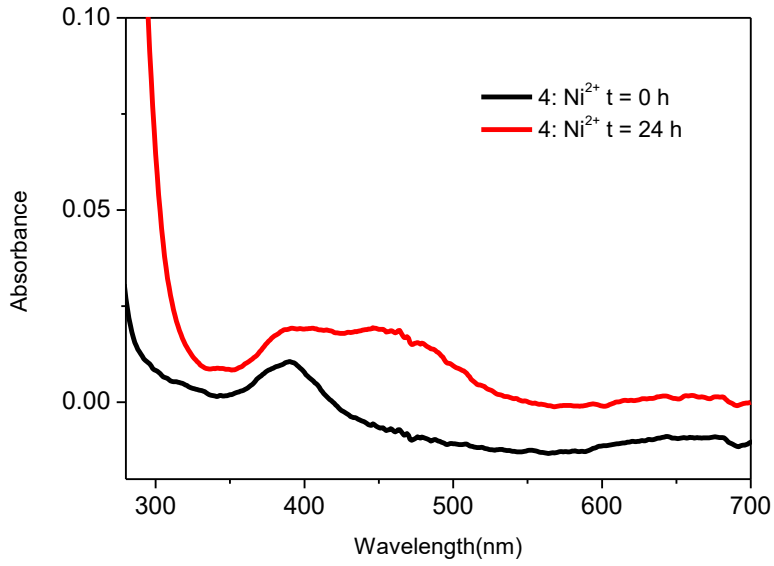

Figure S4. **(a)** UV–Vis spectra for solutions of M^{2+} (2.27 mM in MeOH/H_2O 80/20 v/v) in the presence of 1.2 equivalents of ligand **4** in the absence of added base; **(b)** pictures of vials containing the solutions for spectra in a; **(c)** Same as in *(a)* but after addition of base (see Table S2, ESI for pH values); **(d)** pictures of vials containing the solutions for spectra in *(c)*. **(e)** Comparison of UV-Visible spectra for the Ni^{2+} complex with ligand **4** (t = 0 h and 24 h). 2.5 mM in $Ni(OAc)_2$ and 30 mM in ligand **4** in MeOH/H_2O 80/20 v/v.

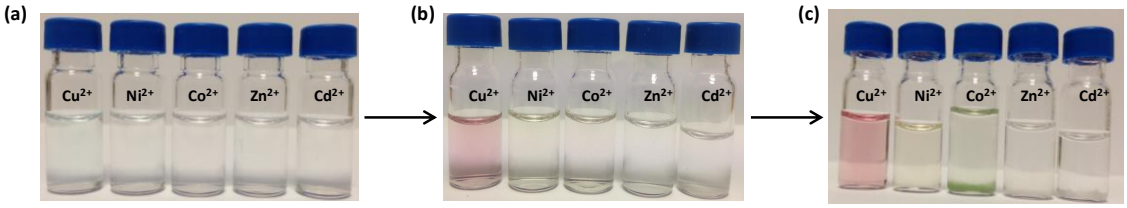

Figure S5. Pictures of vials containing solutions of different metals before and after addition of ligand **4** and base: (a) 2.5 mM solutions of different metal salts in MeOH/H_2O 80/20 v/v; (b) Change of colour upon addition of 1.2 equiv. of the pseudopeptidic ligand; (c) Vials from b after addition of 0.1 M NaOH (2 equiv.).

Table S2. Change in pH of the different M^{2+} and M^{2+}:L solutions

S No	M^{2+}	pH for M^{2+} solution (2.5 mM)	pH for M^{2+}:L (1:1) solution	pH for M^{2+} L (1:1) solution after adding 2 equiv. of 0.1 M NaOH
1	Cu^{2+}	6.0	6.4	9.1
2	Ni^{2+}	6.6	6.7	9.3
3	Co^{2+}	7.2	6.5	9.4
4	Zn^{2+}	7.3	6.2	9.1
5	Cd^{2+}	6.3	7.1	9.8

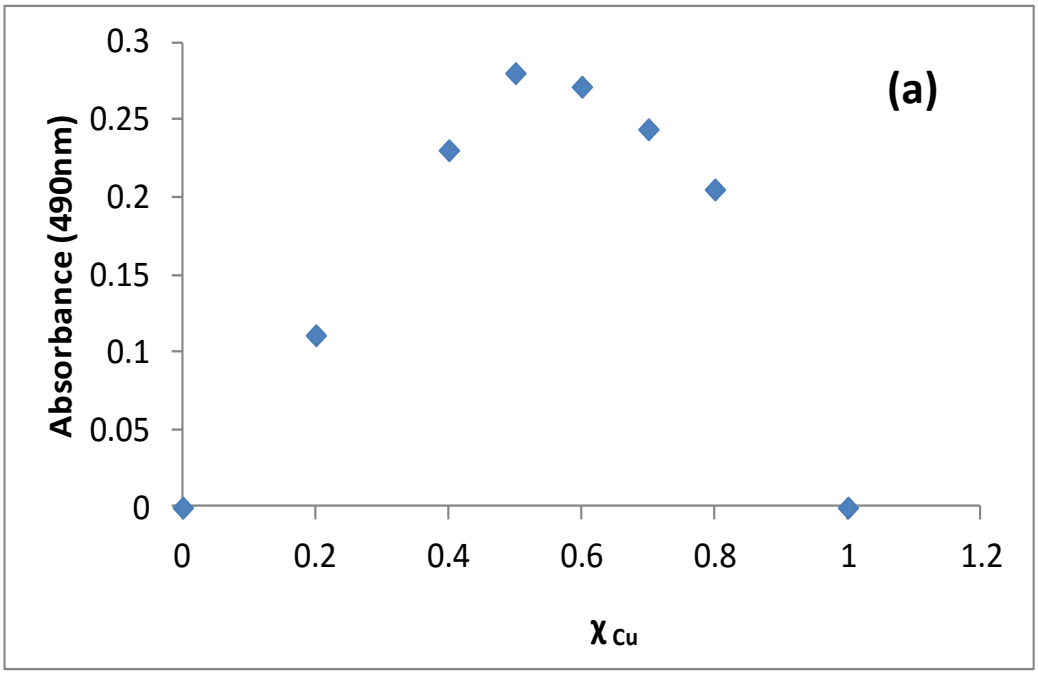

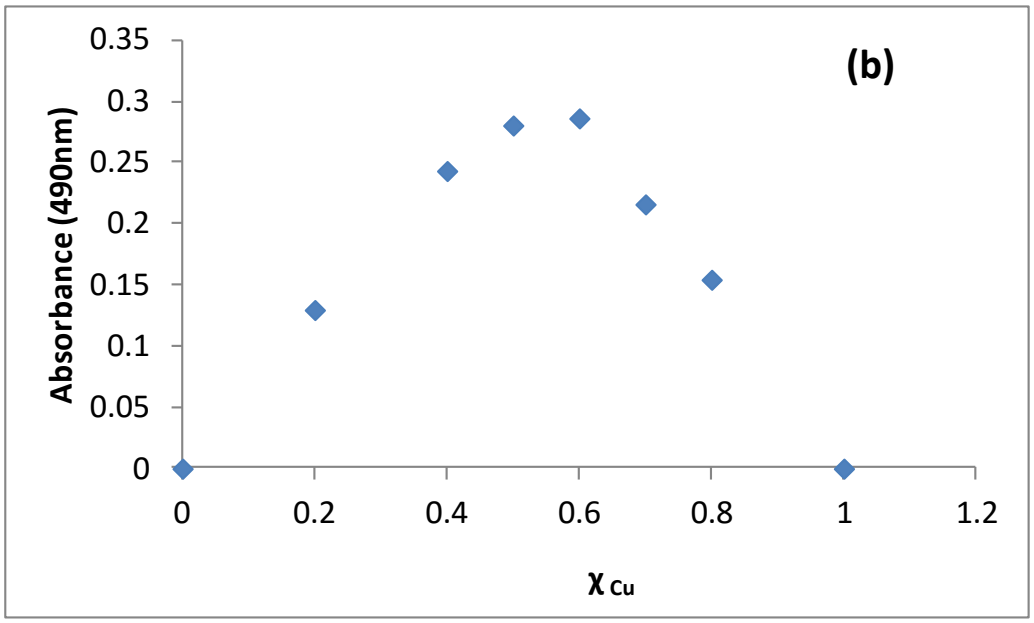

Figure S6. Job plot for ligand **4** (5 mM) and $Cu(OAc)_2$ (5 mM) in MeOH/H_20 80/20 v/v in neutral (a) and basic media (b). Individual measurements were taken after an equilibration period of 5 min, as the complexation needs less than 1 min to be complete. The titration protocol is as follows

1. 1 mL Ligand **4** (5 mM)
2. 800 µL Ligand **4** + 200 µL $Cu(OAc)_2$
3. 700 µL Ligand **4** + 300 µL $Cu(OAc)_2$
4. 600 µL Ligand **4** + 400 µL $Cu(OAc)_2$
5. 500 µL Ligand **4** + 500 µL $Cu(OAc)_2$
6. 400 µL Ligand **4** + 600 µL $Cu(OAc)_2$
7. 300 µL Ligand **4** + 700 µL $Cu(OAc)_2$
8. 200 µL Ligand **4** + 800 µL $Cu(OAc)_2$
9. 1 mL $Cu(OAc)_2$ (5 mM)

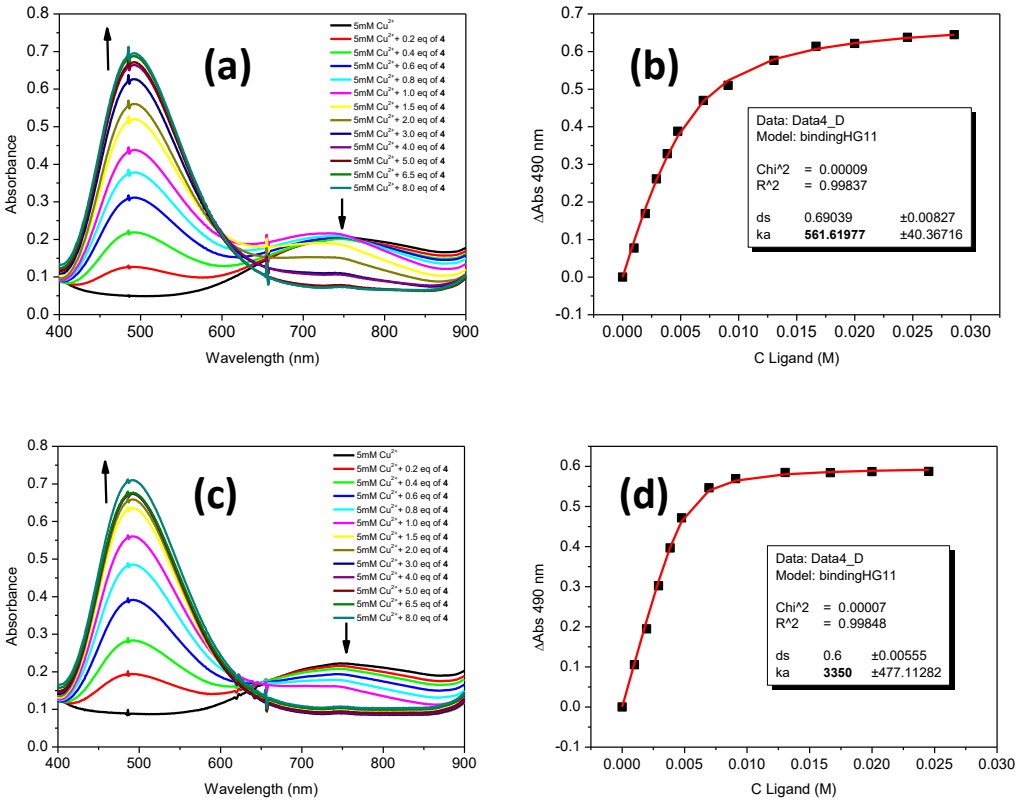

Figure S7. (a) UV-Visible spectra for Cu^{2+} (5 mM in MeOH/H_2O 80:20) in the presence of increasing amounts of ligand **4**. (b) Plot of the absorbance at 490 nm against the concentration of **4**; data for the non-linear fitting have been included; (c) UV-Visible spectra for Cu^{2+} (5 mM in MeOH/H_2O 80:20) in the presence of increasing amounts of compound **4** in basic medium (pH = 11.7). (d) Plot of the absorbance (490 nm) against the concentration of **4**; data for the non-linear fitting in basic media have been included.

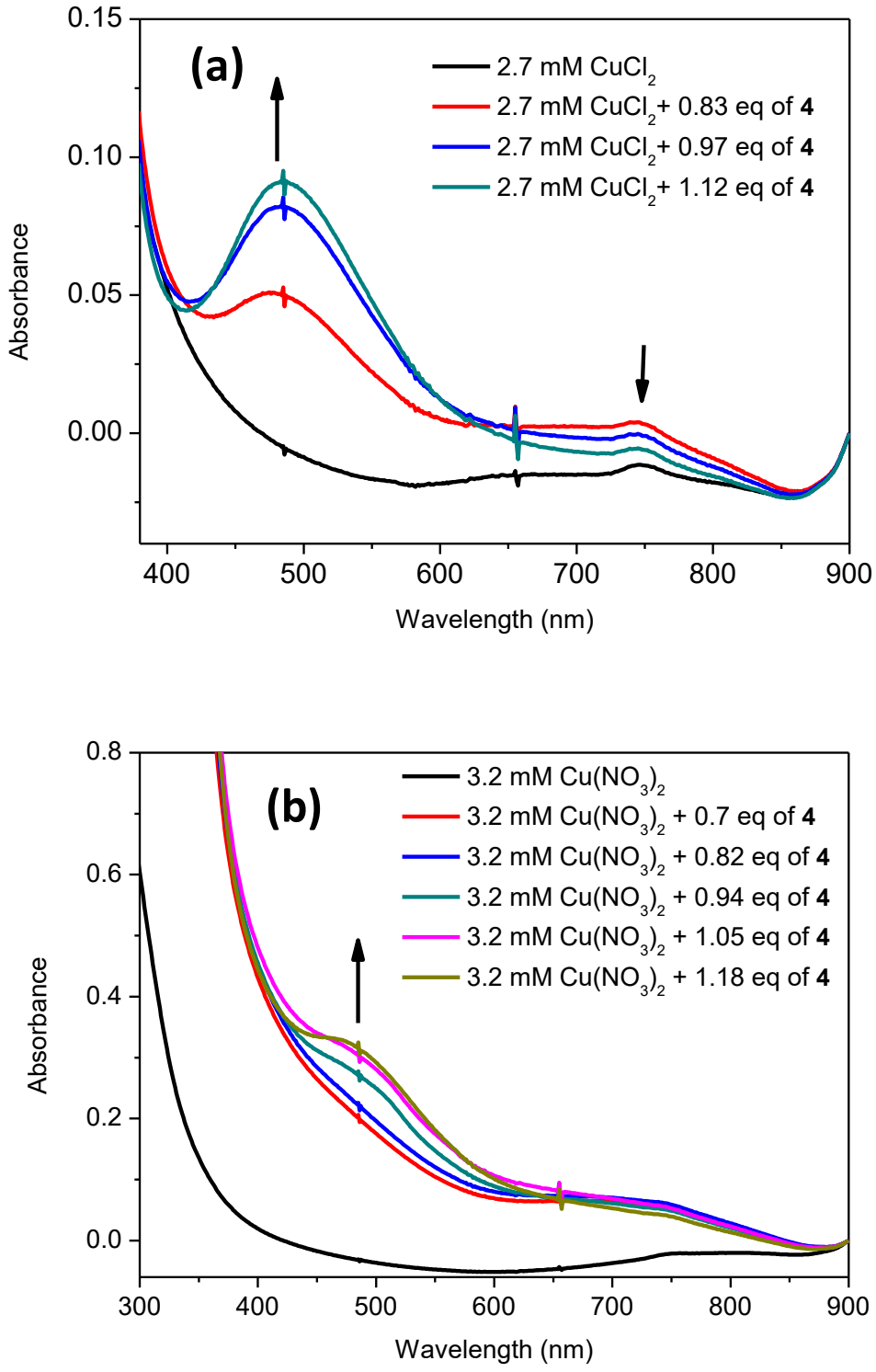

Figure S8. (a) UV-Vis for a solution of $CuCl_2$ (2.7 mM, MeOH/H_2O 80/20 v/v) after addition of variable amounts of **4** (50 mM). (b) UV-Vis for a solution of $Cu(NO_3)_2$ (3.2 mM, MeOH/H_2O 80/20 v/v) for a solution of amounts of **4** (50 mM) in MeOH/H_2O 80/20 v/v.

a)

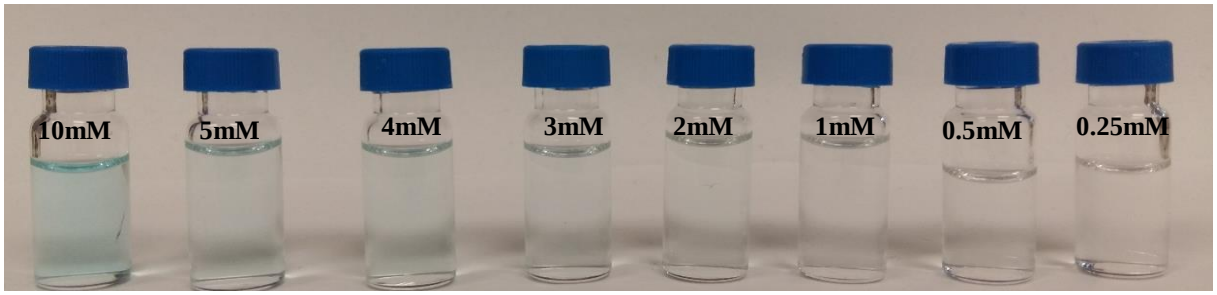

b)

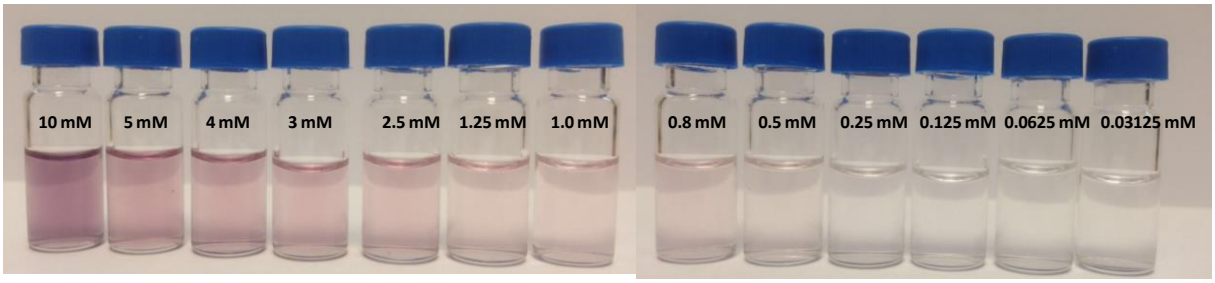

c)

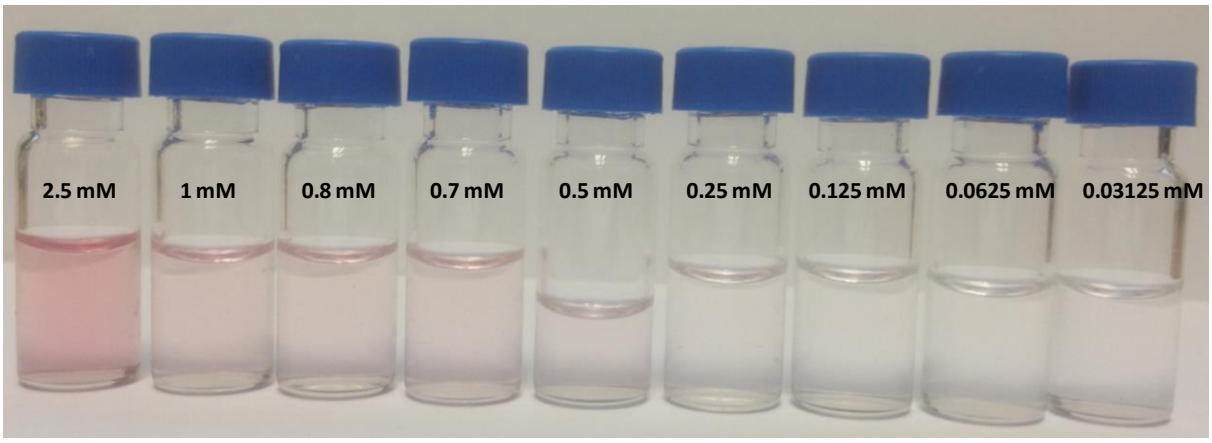

Figure S9. a) Colour changes upon dilution of a solution of $Cu(OAc)_2$. b) Colour changes upon successive dilutions from a 10 mM stock solution of Cu^{2+}:**4** $^{+}$ under neutral conditions. c) Colour changes upon successive dilutions from a 10 mM stock solution of Cu^{2+}:**4** after adding the 2 equiv. of base (0.1 M NaOH in water). The solvent was MeOH/H_2O 80/20, v/v in all cases.

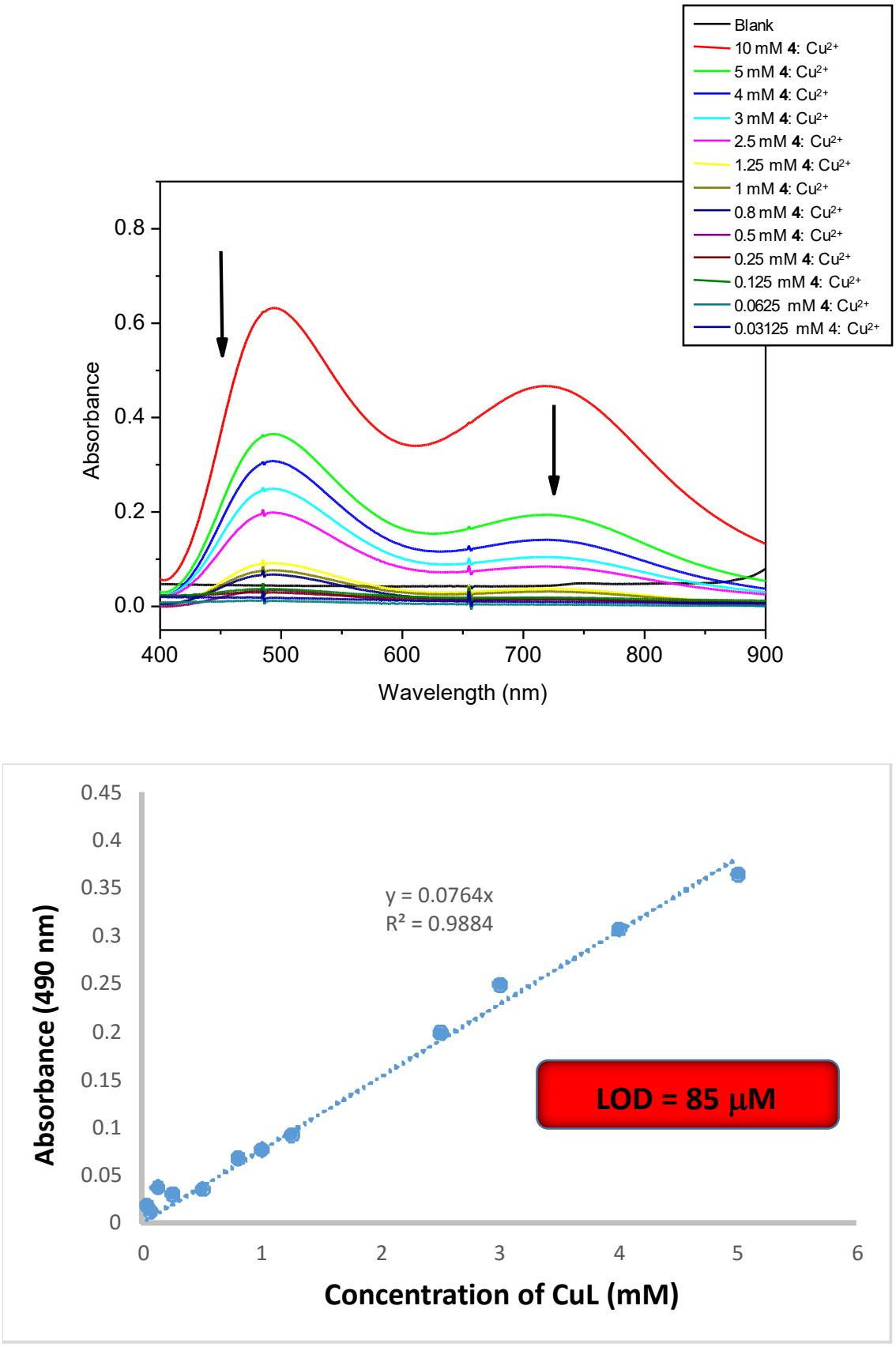

Figure S10. UV-Visible spectra for the Cu^{2+}:**4** complex at different concentrations in MeOH/H_2O 80/20, v/v without added base (top). Plot of the absorbance at 490 nm against the concentration of Cu^{2+}:**4** (bottom).

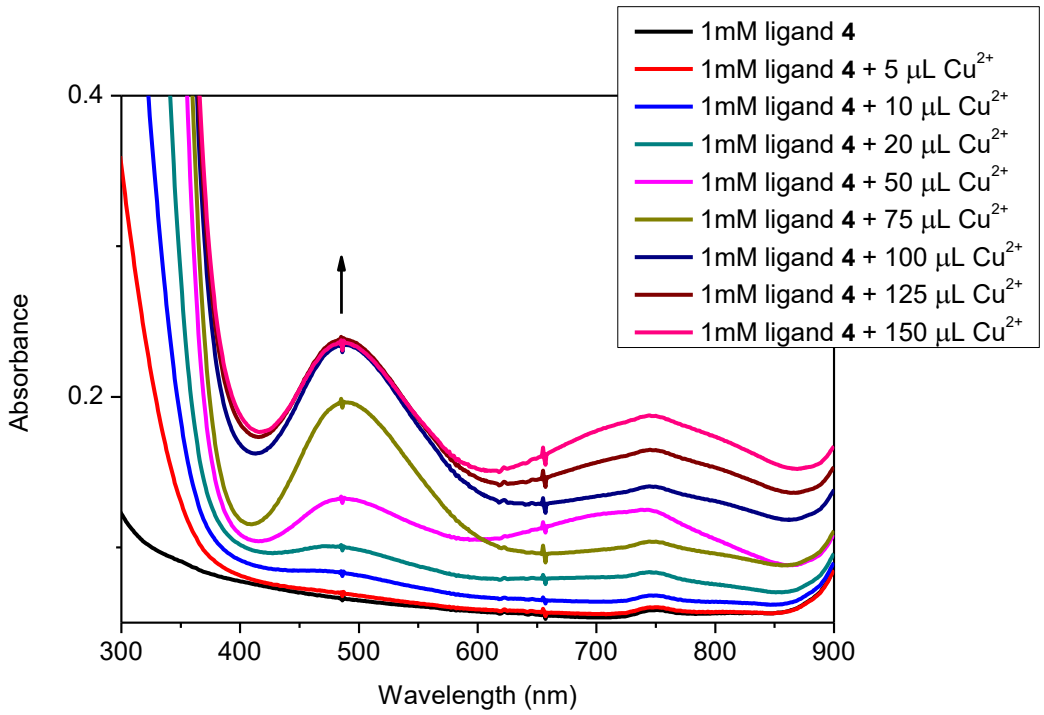

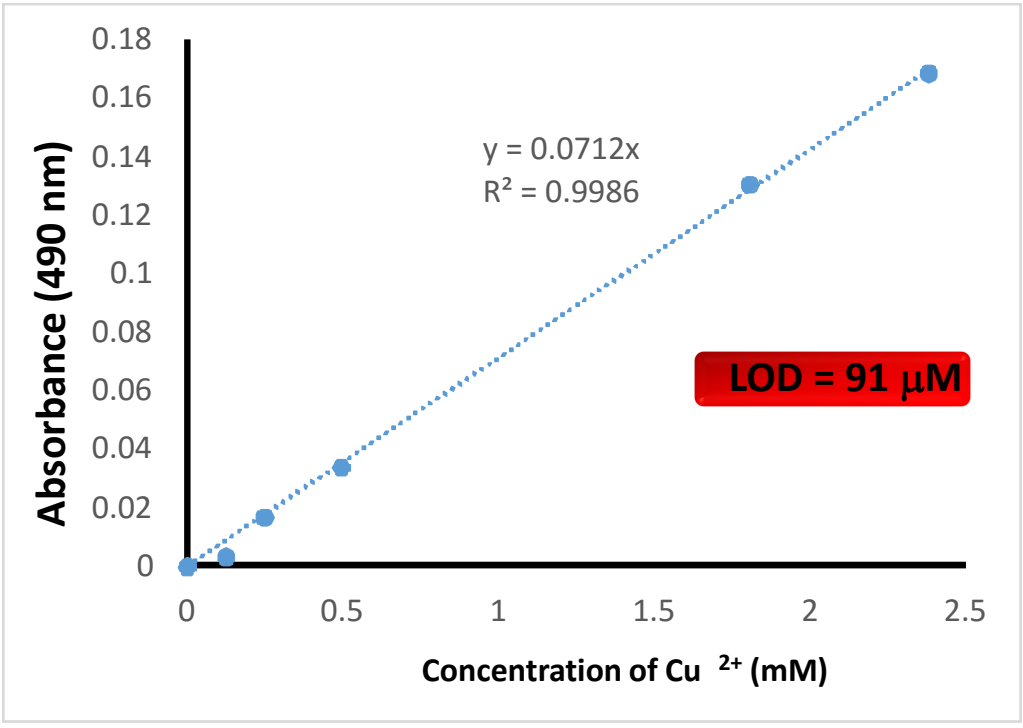

Figure S11. UV-Visible spectra for a solution of ligand **4** (1 mM in MeOH/H_2O 80:20 v/v) after addition of increasing amounts of Cu^{2+} (50 mM) in the absence of base (top). Plot of the absorbance at 490 nm against the concentration of Cu^{2+} (bottom).

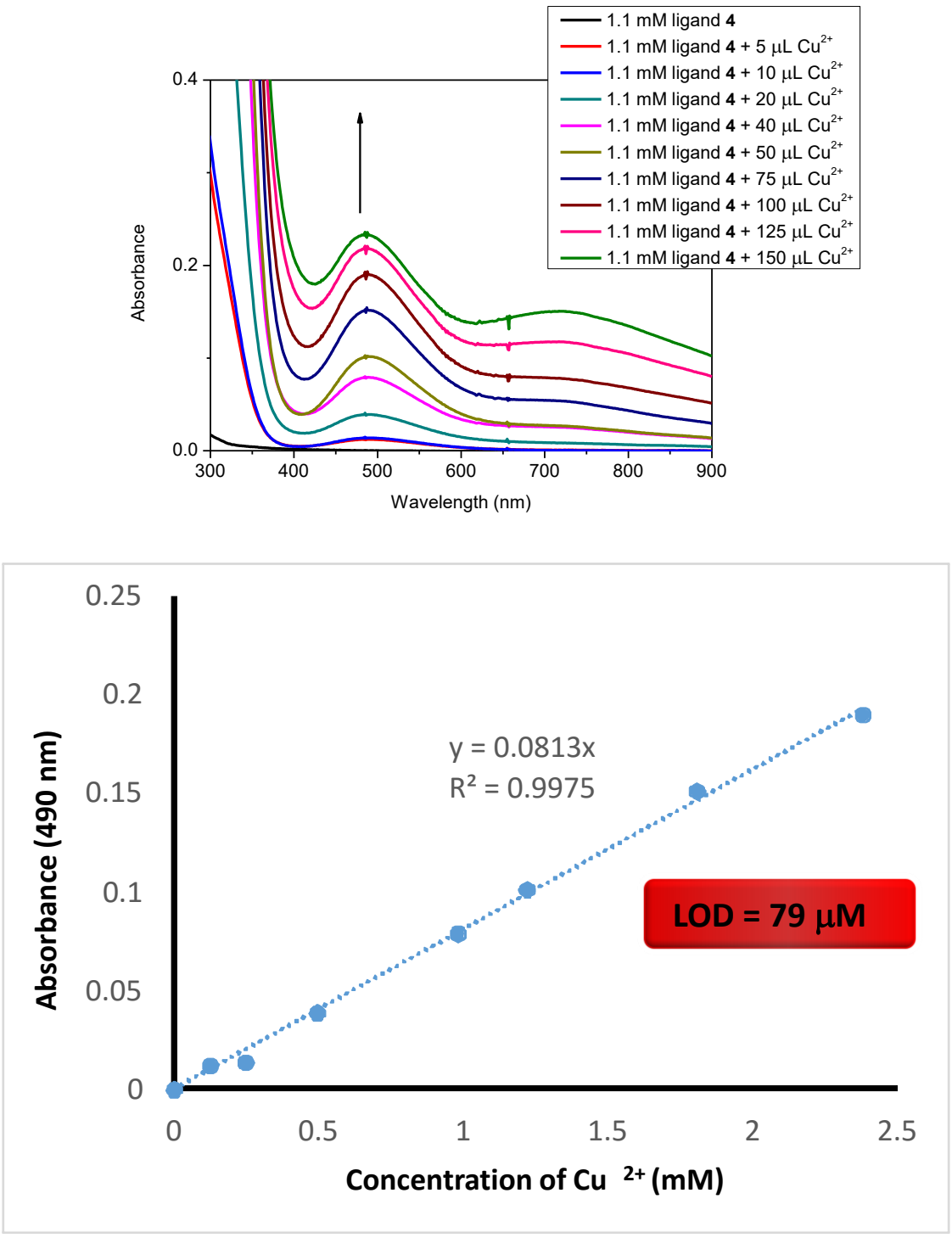

Figure S12. UV-Visible spectra for a solution of ligand **4** (1.1 mM in 0.1 M NaOH in MeOH/H_2O 80:20 v/v) after addition of increasing amounts of Cu^{2+} (50 mM) (top). Plot of the absorbance at 490 nm against the concentration of Cu^{2+} (bottom).

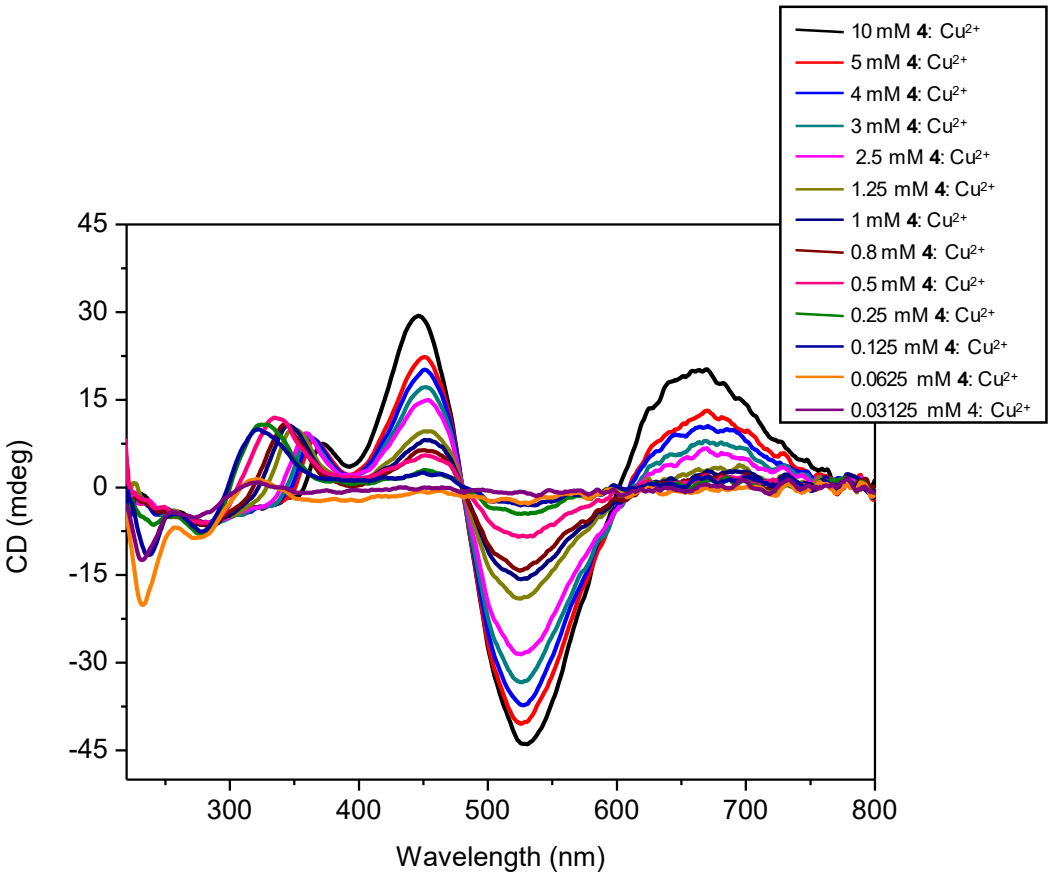

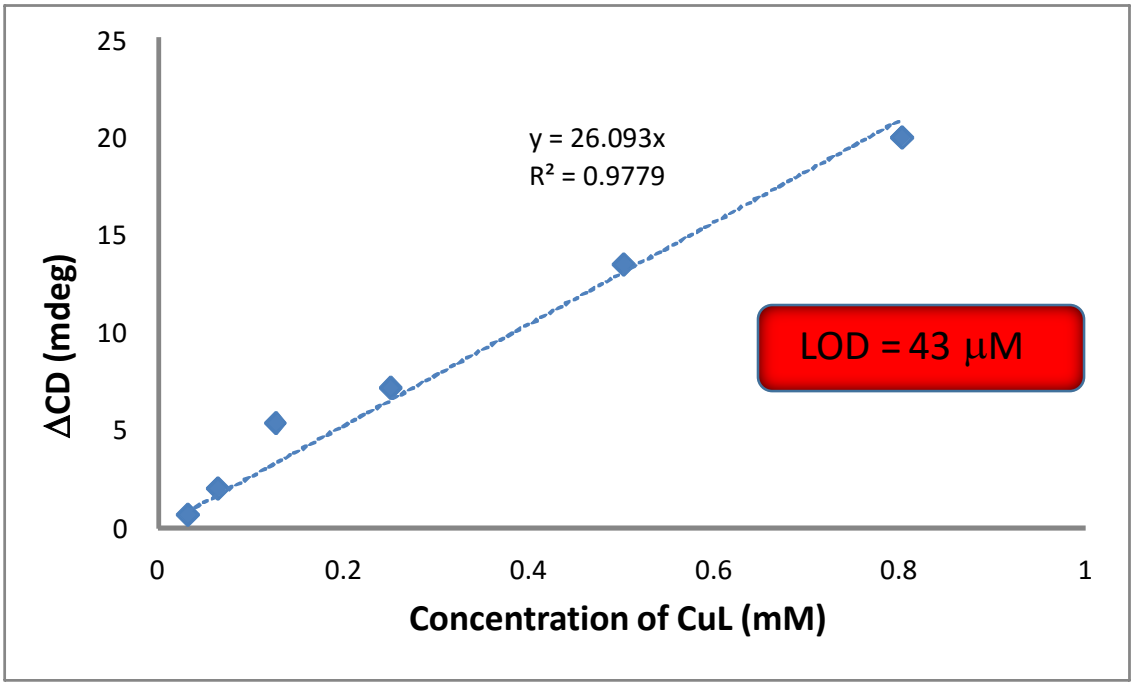

Figure S13. CD spectra for a solution of the Cu^{2+}:**4** complex at different concentrations in MeOH/H_2O 80:20 v/v in the absence of added base (top). Plot of the amplitude of the Cotton effect ($\Delta CD = CD_{440nm}$-CD_{520nm}) against the concentration of Cu^{2+}:**4** (bottom).

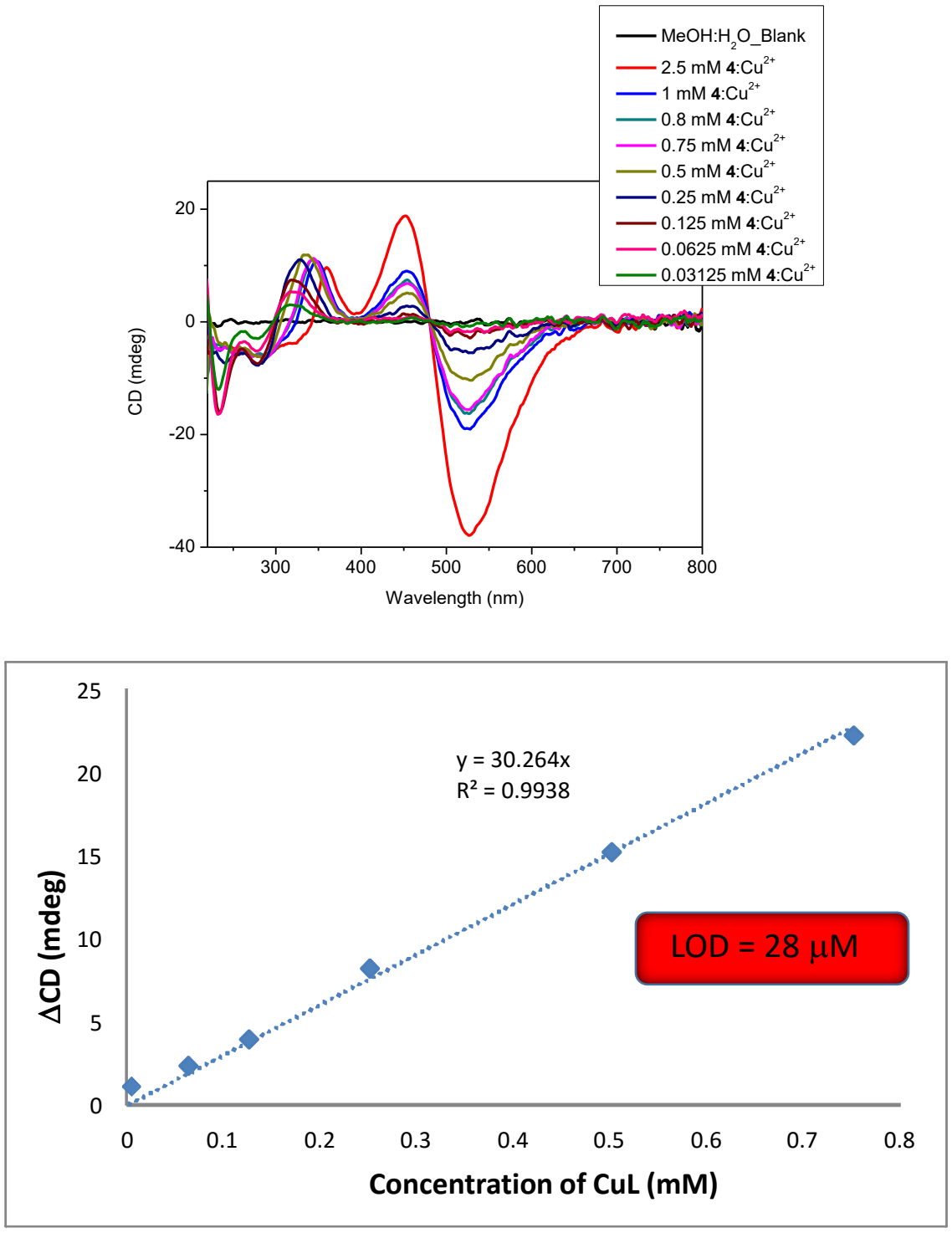

Figure S14. CD spectra for a solution of the Cu^{2+}:**4** complex at different concentrations in MeOH/H_2O 80:20 v/v in the presence of added base 2 eq. (top). Plot of the amplitude of the Cotton effect (ΔCD = CD_{440nm}-CD_{520nm}) against the concentration of Cu^{2+}:**4** (bottom).

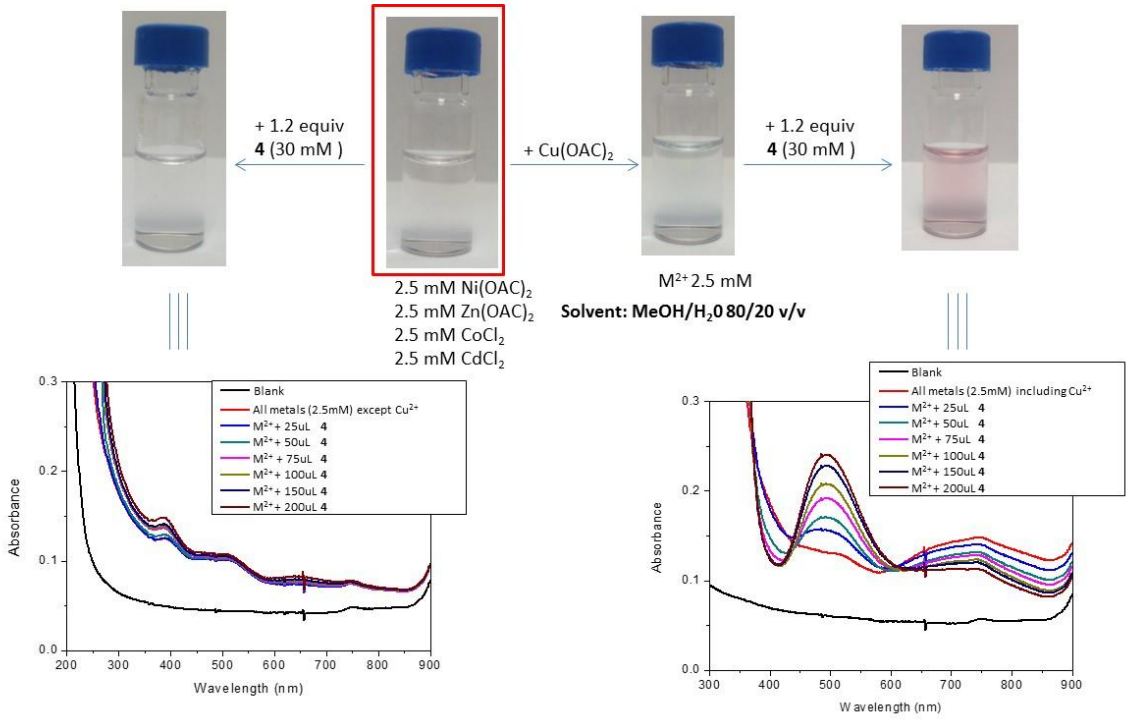

Figure S15. Sensing of Cu^{2+} (2.5 mM, MeOH/H_2O 80/20 v/v) by UV and colour change, in the presence of other metal cations (2.5 mM in each cation) by addition of different amounts of ligand **4** (30mM, MeOH/H_2O 80/20 v/v) in the absence of added base.

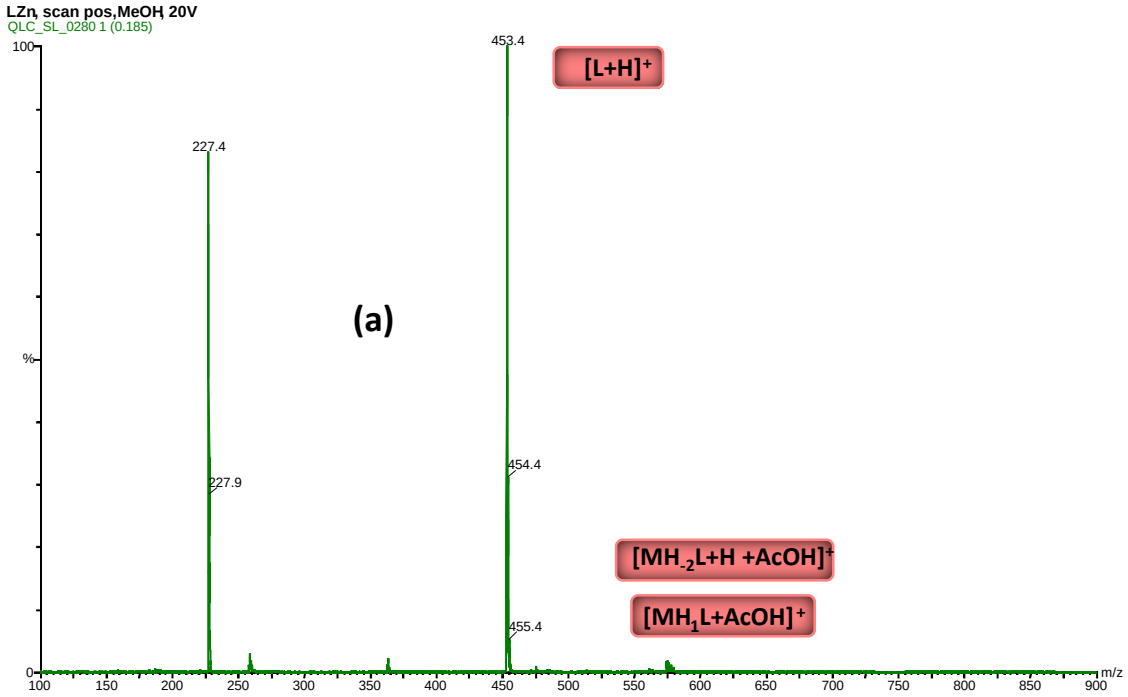
LZn, scan pos,MeOH 20V
QLC_SL_0280 1 (0.185)
100
%
0
453.4
[L+H]+
227.4
(a)
227.9
454.4
[MH-2L+H +AcOH]+
[MH1L+AcOH]+
455.4
100 150 200 250 300 350 400 450 500 550 600 650 700 750 800 850 900
m/z

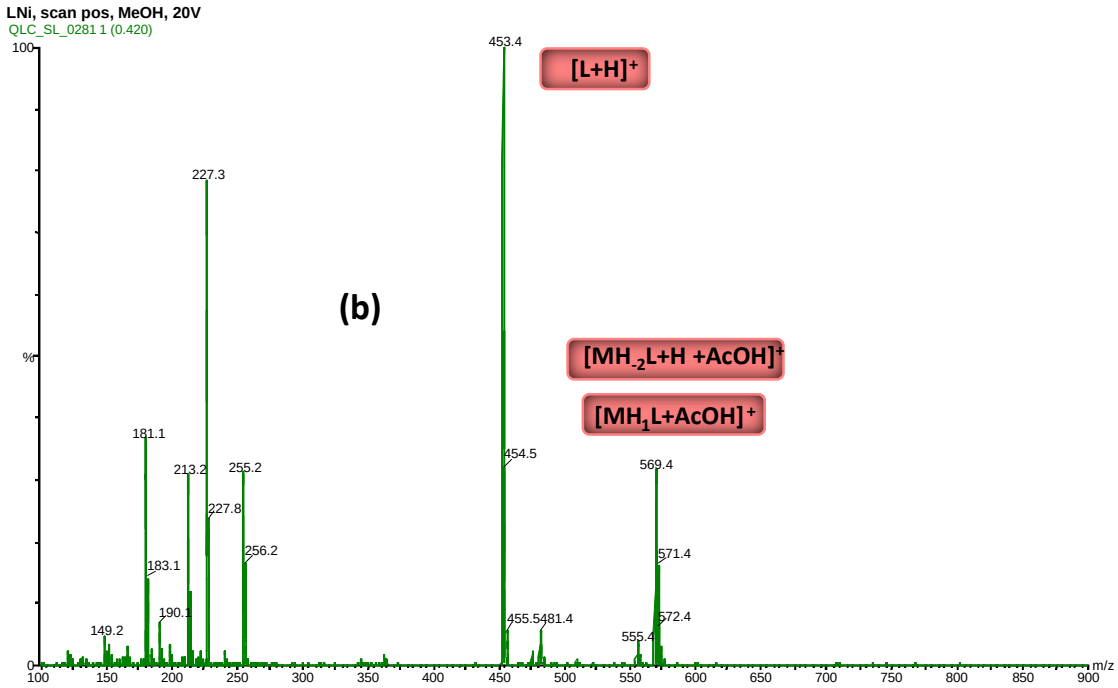
LNi, scan pos, MeOH, 20V
QLC_SL_0281 1 (0.420)
100
%
0
453.4
[L+H]+
227.3
(b)
[MH-2L+H +AcOH]+
[MH1L+AcOH]+
181.1
213.2
255.2
227.8
454.5
569.4
256.2
571.4
183.1
190.1
149.2
455.5
481.4
572.4
555.4
100 150 200 250 300 350 400 450 500 550 600 650 700 750 800 850 900
m/z

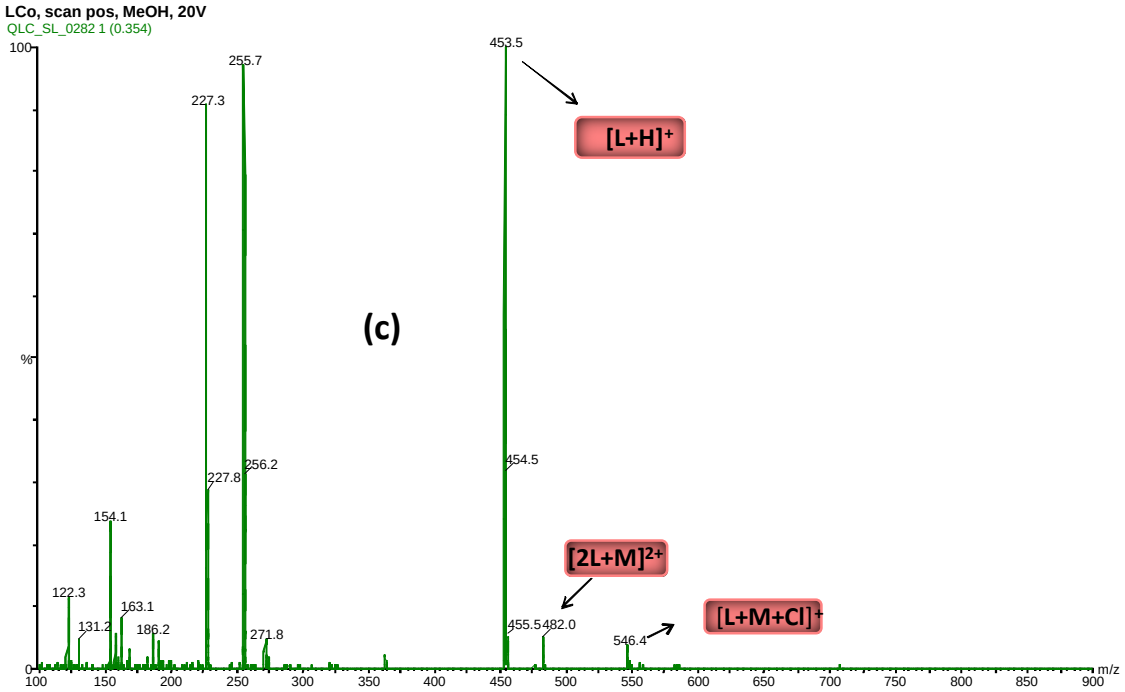
LCo, scan pos, MeOH, 20V
QLC_SL_0282 1 (0.354)
100
%
0
453.5
255.7
227.3
[L+H]+
(c)
454.5
256.2
227.8
154.1
[2L+M]2+
122.3
163.1
131.2
186.2
271.8
455.5
482.0
546.4
[L+M+Cl]+
100 150 200 250 300 350 400 450 500 550 600 650 700 750 800 850 900
m/z

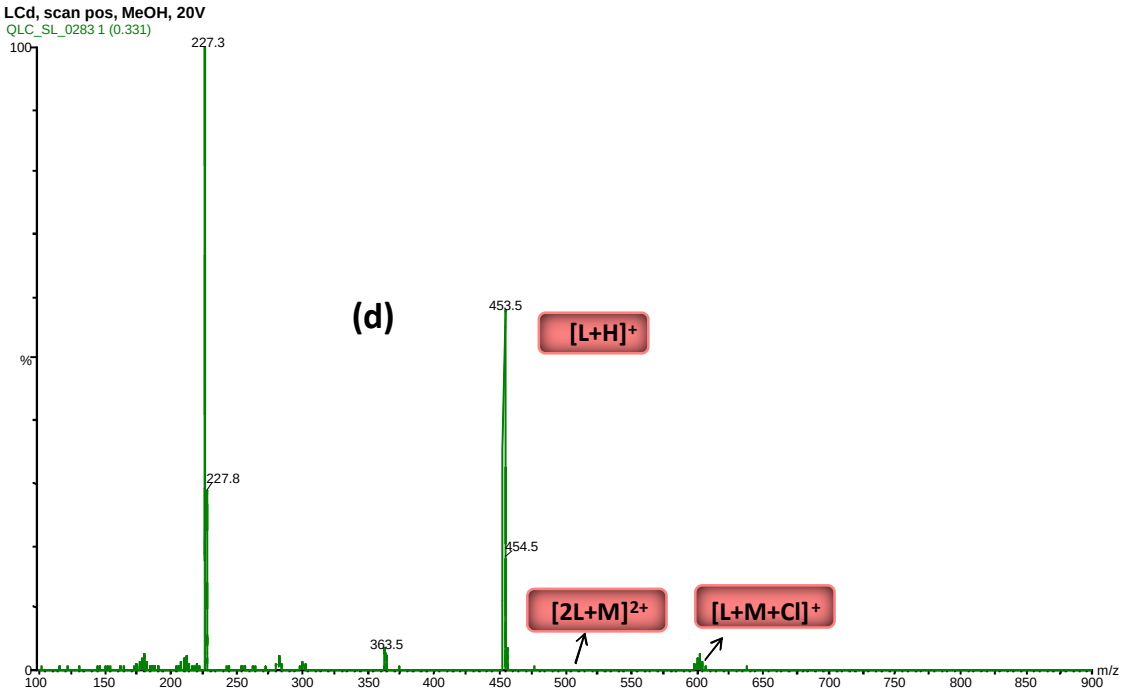
LCd, scan pos, MeOH, 20V
QLC_SL_0283 1 (0.331)
100
%
0
227.3
(d)
453.5
[L+H]+
227.8
454.5
[2L+M]2+
[L+M+Cl]+
363.5
100 150 200 250 300 350 400 450 500 550 600 650 700 750 800 850 900
m/z

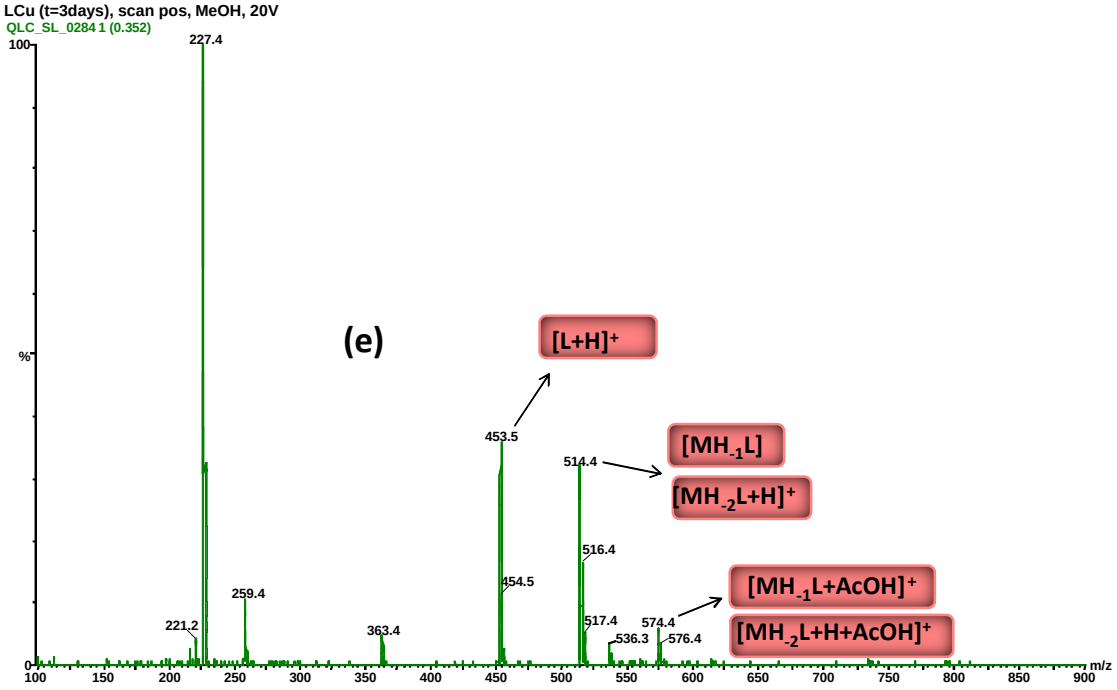

Figure S16. ESI mass spectra for ligand **4** (2.5 mM) in the presence of equimolecular amounts of different metals in MeOH/H_2O 80/20 v/v. a) Zn^{2+}; b) Ni^{2+}; c) Co^{2+}; d) Cd^{2+}; e) Cu^{2+} after 48 hours.

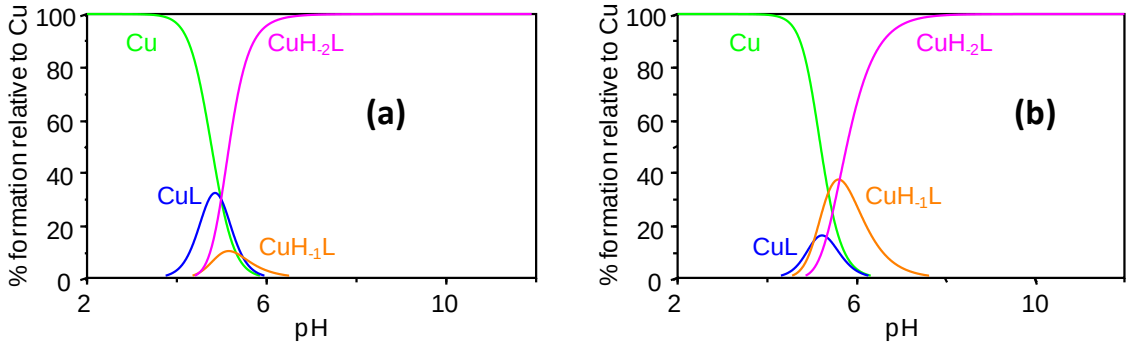

Figure S17. Distribution diagrams for the systems involving ligands **2** (a) and **4** (b) and Cu^{2+} (1:1 stoichiometry) as a function of pH in 0.1 M NaCl in H_2O/CH_3CN 7/3 v/v, at 298.1 ± 0.1 K. Charges have been omitted for clarity.